IOP Publishing Physiol. Meas. 42 (2021) 054003 https://doi.org/10.1088/1361-6579/abfb0a

Physiological Measurement

IPEM Institute of Physics and Engineering in Medicine

OPEN ACCESS

RECEIVED
14 January 2021

REVISED
16 April 2021

ACCEPTED FOR PUBLICATION
23 April 2021

PUBLISHED
17 June 2021

PAPER

Investigating the role of pericytes in cerebral autoregulation: a modeling study

Selena Milanovic[1], **Kira Shaw**[2], **Catherine Hall**[2] **and Stephen Payne**[1]

[1] Institute of Biomedical Engineering, University of Oxford, Oxford, United Kingdom
[2] School of Psychology, University of Sussex, Brighton, United Kingdom

E-mail: selena.milanovic@stx.ox.ac.uk

Keywords: pericytes, CBF regulation, autoregulation, haemodynamic, mathematical modeling

Abstract

The brain's inability to store nutrients for more than a few seconds makes it one of the most tightly regulated systems in the body. Driven by metabolic demand, cerebral autoregulation (CA) ensures a constant cerebral blood flow (CBF) over a ±50% change in arterial blood pressure (ABP) from baseline. Recent evidence suggests that pericytes, contractile cells in the capillary bed, play a previously-ignored regulatory role. To elucidate the CA phenomenon, the role of oxygen metabolism, pericyte activity and neural signaling in CBF modulation were quantified. Driven by nutrient metabolism in the tissue and pressure sensitivity in the vasculature, the model introduced here successfully replicates CA. To highlight the role of different vessel sizes, vessels with a diameter above 1 mm were represented using a lumped parameter model while the microvasculature was illustrated as a branching tree network model. This novel approach elucidated the relationship between the microvasculature's nutrient supply and arterial regulation. Capillary responses to local increases in neuronal activity were experimentally determined, showing that pericytes can increase the diameter of the adjacent vessel by 2.5% in approximately 1 s. Their response was quantified and included in the computational model as an active component of the capillary bed. To compare the efficacy model presented here to existing ones, four feedback mechanisms were tested. To simulate dynamic CBF regulation a 10% increase in ABP was imposed. This resulted in a 23.79%–34.33% peak increase in CBF, depending on the nature of the feedback mechanism of the model. The four feedback mechanisms that were studied significantly differ in the response time, ultimately highlighting that capillaries play a fundamental role in the rapid regulation of CBF. Conclusively, this study indicates that while pericytes do not greatly alter the peak CBF change, they play a fundamental role in the speed of regulation.

1. Introduction

To ensure an adequate tissue perfusion, the brain relies on a tightly regulated system of vessels. Both large and small, each vessel category has a specific and indispensable function. Arteries operate at the highest blood pressure, regulating flow through a smooth muscle cell (SMC) driven compliance (Cipolla 2016). Capillaries penetrate the white matter and supply the tissue with nutrients through a network of predominantly bifurcating vessels (Cassot and Lauwers 2006). Ultimately, nutrient-poor blood flows back to the heart through a series of veins and sinuses.

Being highly sensitive to perfusion changes, the brain relies on an autoregulation mechanism, driven by an active response of the arteries and arterioles. The regulatory drivers differ in nature, being either global (i.e. set by the systemic circulation) or local (i.e. set by changes in metabolic demand) (Payne 2006, 2016). Global and local regulating mechanisms are interlinked and changes in one therefore result in an alteration in behavior of the other. Sometimes these mechanisms compensate for each other's deficiency, yet the magnitude of their importance of governing agents is yet to be defined.

Nutrient supply takes place in the microvasculature of the brain, targeting the capillary network. Pericytes, contractile cells found on capillary vessels, have been recently proved to actively regulate capillary vessel diameter (Burdyga and Borysova 2014). A dysfunction in this further regulating mechanism is linked to several pathological conditions (Hall *et al* 2014, Attwell *et al* 2016).

Numerous studies (Hall *et al* 2014, Sweeney *et al* 2019) support the notion that sufficient tissue perfusion is essential for a healthy brain function. Indeed, low cerebral blood flow (CBF) has been associated with dementia onset and tissue atrophy. Alzheimer's disease is also linked to a lack of tissue perfusion, underlining the importance of adequate oxygenation levels (Sweeney *et al* 2019). Neurons are particularly susceptible to drops in oxygen supply, as almost 75% of the brain's energy supply is consumed by the neural network (Bélanger *et al* 2011). Low levels of partial tissue pressure are characteristic of several ischemic conditions, such as stroke and neurogenesis (Hall *et al* 2014).

Imaging alone has proven to be an insufficient tool when investigating the mechanisms of CBF regulation within the microvasculature, as human imaging data are restricted to a resolution of order 1 mm (Wintermark *et al* 2005, Cheng *et al* 2017). Mathematical models therefore represent a suitable approach for investigating the coupling between flow and metabolism which occurs at the microvasculature length scale. Here, a metabolic demand-driven model on the arteriole scale was coupled with a pericyte activity-driven one on the capillary scale.

Metabolism is considered one of the key drivers of vasodilation (Reglin *et al* 2009, Bulte *et al* 2012) with oxygen partial tissue pressure acting as a modulator of arterial compliance. Furthermore, the activity of pericyte cells was represented as a dilation of the capillary vessels, further contributing to an active regulation of CBF. Ultimately, neural activity was introduced to emulate a fast vasoreactivity, resulting in a brain vasculature model whose time response for dynamic changes of CBF faithfully represents reality.

To achieve this, a microvasculature network of arterioles, capillaries and venules was coupled with a lumped parameter model of large arteries and veins. This resulted in a model of the complete brain vasculature whose local and global responses were analyzed. The activity of pericytes, defined by a variable capillary diameter in the model, was derived from experimental data on capillary diameter variation in mice. Finally, the time response of the model to changes in pressure was analyzed, aiming to disentangle the individual and cumulative role of the proposed CBF regulators.

2. Methods

With the aim of designing a physiologically representative CBF regulation mechanism, the computational model presented here comprises two parts: the first part consists of large arteries and veins whose response is modeled through an electrical equivalent model while the second part extrapolates from experimental data on pericyte-induced dilation, which are included in a microvasculature network model. Figure 1 is a representation of the multi-scale model proposed here.

To quantify the model's efficacy to mimic dynamic CBF regulation in a physiologically accurate way, it was compared to the frequently cited flow-feedback model. Precisely, four feedback mechanisms were defined and compared with each other: a flow feedback (F_0), an oxygen feedback (F_1), an oxygen and pericytes feedback ($F_1 + F_2$), and an oxygen, pericytes and neural feedback ($F_1 + F_2 + F_3$) mechanism.

2.1. Experimental model

Pericyte responses to local increases in neuronal activity were experimentally determined using two-photon imaging of the visual cortex in awake mice (C57BL/6J background) expressing a genetically encoded calcium (Ca^{2+}) indicator in excitatory neurons and with the vascular lumen labeled with injected Texas Red dextran. To induce neural activity in the mice, a visual stimulus (i.e. virtual maze) was presented, which resulted in an increase in Ca^{2+} in the active brain region. A detailed outline of the procedure is presented by Shaw (2019). Two distinct sets of data were used for the experimental part of the study, as changes in diameter and cerebral metabolic rate of oxygen ($CMRO_2$) cannot be assessed simultaneously. Indeed, to measure the net cerebral blood flow and hemoglobin oxygenation a parallel set of experiments (using 36 vessels) was performed using a probe (VMS Oxy, Moor Instruments) that combines laser doppler flowmetry and hemoglobin spectrometry. On the other hand, to measure pericyte-induced vessel dilation, 26 capillaries were imaged using a two-photon microscopy objective.

2.1.1. Pericyte induced capillary dilation

To study the diameter change induced by pericyte activity, a total of 26 capillary vessels from 6 mice were considered. Ranging between 2 and 13 μm in diameter (see figure 2), the vessels were studied at imaging depths between 0 and 350 μm. A Ca^{2+} stimulus lasting 5 s was applied 10–12 times to each vessel with intervals of 10 s

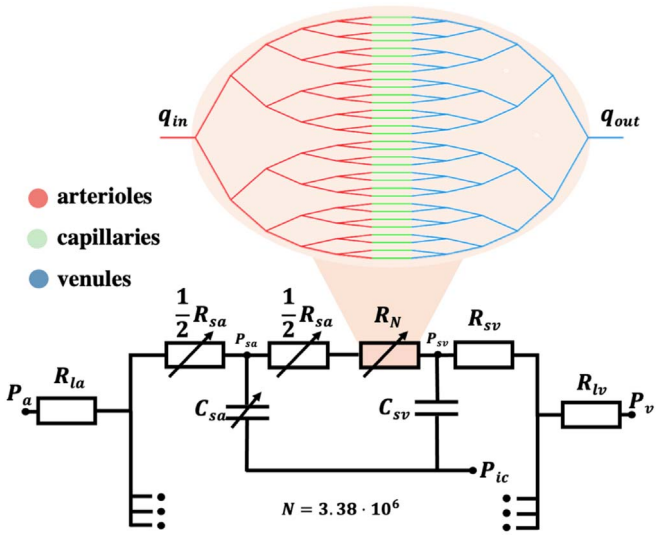

Figure 1. Schematic representation of the haemodynamic model. A network model representing the behavior of 6 arteriole generations (red), 1 capillary bed (green) and 6 venule generations (blue) is incorporated in a lumped parameter model whose elements reflect the behavior of larger arteries and veins.

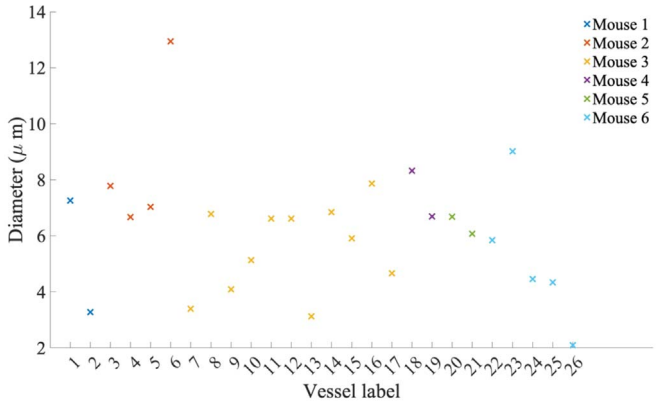

Figure 2. Baseline diameters of all capillary vessels. A total of 26 vessels was obtained from 6 mice, each highlighted with a different color.

(see figure 3(a)). This process was repeated 3–8 times for each of the 26 vessels. Both the local Ca^{2+} trace (see figure 3(b)) and the diameter trace (see figure 3(c)) of each vessel were tracked.

2.1.2. Capillary selection

From the total number of vessels used for the experiment, the behavior of 8 vessels was included in the computational study following two exclusion principles. The first exclusion factor for the data was vessel diameter. An acceptable range of 6–10 μm was established, as the capillary diameter defined within the capillary network of the mathematical model presented here is 8 μm. Figure 4(a) presents the average response for all 26 vessels, while figure 4(b) presents the response of the selected eight vessels. As defined in the literature (Payne and Lucas 2018), vessels above the established threshold (>8 μm) are categorized as arterioles while those below are most often dead-end vessels.

The second selection criterion was the vessel's responsiveness to Ca^{2+} stimuli (i.e. non-responsive vessels, defined by a coefficient of variance <1% of the diameter change, were ignored). See table A1 in the appendix for a comprehensive overview of the responsiveness of each vessel.

2.1.3. Diameter trace fitting

The fitting function was solved in the s-domain using the Laplace transform and subsequently converted back to the time domain. The first step was to define the Ca^{2+} stimulus on which the function is based. This was modeled as a rectangular pulse function $x(t)$ with width $T = 5$ s, as that corresponds to the duration of the Ca^{2+}

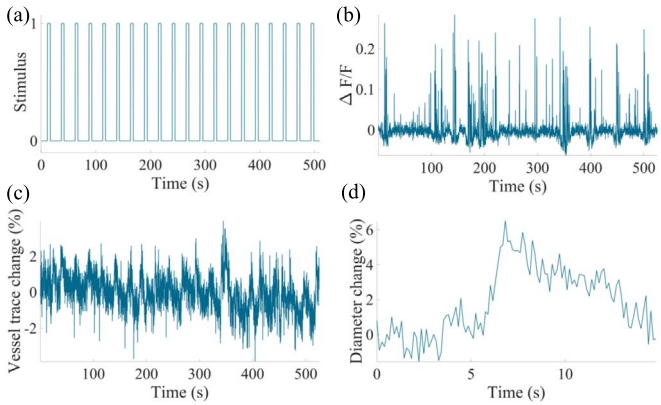

Figure 3. Example of data processing for Vessel 1 (a) Ca^{2+} stimulus intervals; (b) Ca^{2+} trace over time; (c) normalized vessel trace over time; (d) ensemble average of diameter change.

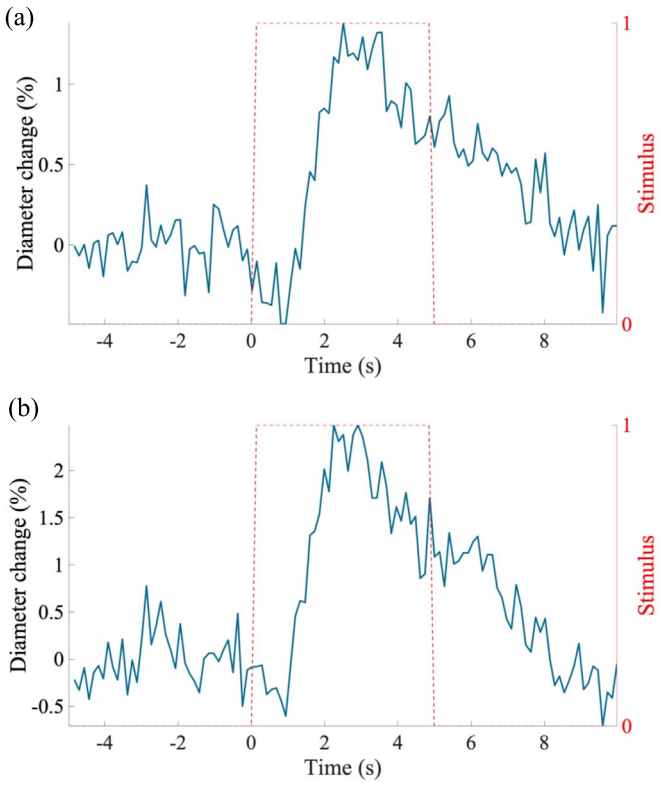

Figure 4. Averaged capillary diameter response to a 5 s Ca^{2+} stimulus for (a) all 26 and (b) 8 selected vessels.

stimulus:

$$x(t) = u(t) - u(t - T), \tag{2.1}$$

where $u(t)$ is a Heaviside function. Being an overshoot function, the model fit was then evaluated from a standard second order model as follows:

$$F(s) = \frac{K(s + \alpha)}{s(s + \beta)(s + \gamma)}, \tag{2.2}$$

where α, β, γ and K are time constants. The inverse Laplace transform of $F(s)$ is $f(t)$ and combined with the stimulus equation $x(t)$ defines the fitted function $y(t)$:

$$y(t) = u(t)f(t) - u(t - T)f(t - T). \tag{2.3}$$

2.1.4. Oxygen metabolism

With the aim of relating pericyte cell activation to an increase in nutrient metabolism within the tissue, the Ca^{2+} stimuli were subsequently related to the $CMRO_2$, which was calculated from CBF and the level of deoxyhaemoglobin (Hb_d) and the total level of hemoglobin (Hb_T):

$$\mathrm{CMRO_2} = \mathrm{CBF}\,\frac{\mathrm{Hb}_d}{\mathrm{Hb}_T}. \tag{2.4}$$

When 5 s visual stimuli were presented, $CMRO_2$ increased in visual cortex in 36 out of 46 recordings. The 10 unresponsive recordings were excluded from further analysis.

2.2. Computational model

The model presented here incorporates a network model in a lumped parameter one (see figure 1). An advantage of such coupled models is their ability to relate local changes in tissue oxygenation levels to blood flow. This was achieved through the implementation of a microvasculature network that comprises vessels with diameters ranging from few μm to hundreds of μm. Indeed, oxygen diffusion from vessels to tissue occurs over several different vessel generations. At the inlet of the first vessel generation, oxygen saturation is as high as 95%, subsequently declining to approximately 75% upon entry in the capillary bed and reaching a concentration as low as 55% upon entry in the venous bed (Payne and Lucas 2018).

The driving component of the active blood flow regulation process was set to be the cumulative effect of capillary vasodilation and the compliance of small arteries. With the aim of comparing the novel model presented here with currently existing ones, the model's response to arterial pressure changes was examined under four conditions: compliance based on changes in flow, oxygen sensitivity alone, added pericyte activity and ultimately the influence of neural activation. The flow-driven compliance is a common approach of CBF modeling, yet it has very little physiological grounding. Therefore, the remaining three approaches aim to reproduce the same results but using an anatomically more accurate feedback mechanism.

With the aim of highlighting the differences between these four modeling approaches, a comparison of the models is presented here under static and dynamic conditions. This enabled the quantification of the individual and coupled effect of oxygen sensitivity and pericyte activity highlighting the potential contribution of both to an active CBF regulation.

2.2.1. Electrical equivalent

The computational model introduced here is a multi-scale representation of the complete brain vasculature. As shown in figure 1, large vessels are represented by lumped parameters while the microvasculature is studied through a network model. The varying compliance and resistance of the network (of small arteries and capillaries) are denoted with an arrow. The series of small vessels is repeated in parallel, generating a complete brain model. Following an approach analogous to the one described by numerous authors (Ursino and Lodi 1997, Ursino *et al* 1998, Banaji *et al* 2005) the elements of the circuit are: P_a arterial pressure; R_{la}resistance of large arteries; R_{sa} resistance of small arteries; R_N resistance of microvasculature bed; R_{sv} resistance of small veins; R_{lv} resistance of large veins; P_v venous pressure; q_{in} and q_{out} are the in- and out-flow of the microvasculature; P_{sa} and P_{sv} are nodal pressures. A complete description of the parameters' baseline values is provided in table A2 in the appendix.

The arterial compartment comprises regulating small arteries R_{sa} and non-regulating large arteries R_{la}. Hence, the large vessels are assumed to have a constant resistance and volume whilst those of the small vessels are variable. This is justified by the common assumption that it is primarily small arteries and arterioles that govern active regulation.

The capillary vessels of the microvasculature are assumed to have a variable diameter leading to a variable network resistance R_N. The venous compartment is composed of small veins R_{sv} and large veins R_{lv}; the values of resistance are constant yet the venous volume changes through its compliance C_v. ICP is assumed to be constant at 10 mmHg here, in accordance with existing models (Payne 2006, Bessonov *et al* 2016).

In order to provide a model of the entire cerebral vasculature, the series of resistors and capacitors was duplicated N times. This scaling factor $N = 3.38 \cdot 10^6$ was obtained by calculating the ratio between the baseline value of CBF ($\bar{q} = 12.5$ ml s^{-1}) and blood flow at the entrance of the microvasculature network ($\overline{q_N} = 3.7 \cdot 10^{-6}$ ml s^{-1}), as shown in:

$$N = \frac{\bar{q}}{\overline{q_N}}, \tag{2.5}$$

where $\overline{q_N}$ was calculated following Poiseuille's law:

$$\overline{q_N} = \frac{\Delta P}{R}. \tag{2.6}$$

The baseline value of the total resistance of the microvascular network ($\overline{R_N} = 2.98 \cdot 10^{-5}$ mmHg $\cdot$ s/ml) was represented as the sum of all the resistances of each of the 13 generations:

$$R_N = \sum_{i=1}^{13} R_i. \tag{2.7}$$

Dynamic changes in flow were calculated as described in Payne and El-Bouri (2017). This formulation of flow calculation was designed particularly for dynamic changes in flow in vessels whose diameter is smaller than 1 mm. Therefore, inlet and outlet flow were calculated for each generation using the following equations:

$$\begin{pmatrix} q_{\text{in}} \\ q_{\text{out}} \end{pmatrix} = \alpha_0 \begin{pmatrix} p_{\text{in}} \\ p_{\text{out}} \end{pmatrix} - \frac{r^2}{\nu} \alpha_2 \frac{d}{dt} \begin{pmatrix} p_{\text{in}} \\ p_{\text{out}} \end{pmatrix}, \tag{2.8}$$

$$\alpha_0 = \frac{1}{R} \begin{pmatrix} 1 & -1 \\ 1 & -1 \end{pmatrix}, \tag{2.9}$$

$$\alpha_2 = \frac{1}{6R} \begin{pmatrix} 1 & -1 \\ 1 & -1 \end{pmatrix} + \frac{4\beta}{3R} \begin{pmatrix} -2 & -1 \\ 1 & 2 \end{pmatrix}, \tag{2.10}$$

$$\beta = \frac{\nu RC}{8r^2}, \tag{2.11}$$

where ν is the kinematic viscosity. Under dynamic conditions, the formulation of blood volume is defined as:

$$V_b = \frac{C}{2}(p_{\text{in}} + p_{\text{out}}), \tag{2.12}$$

with conservation of blood volume yielding the change in V_b as the difference between inlet and outlet flow.

2.2.2. Governing equations

The governing equations of the model were based on the relationships described by Payne (2006). Blood vessel resistance varies with the fourth power of its radius, while vessel volume varies with the square of the radius, giving:

$$\frac{V_{\text{sa}}}{\overline{V_{\text{sa}}}} = \sqrt{\frac{\overline{R_{\text{sa}}}}{R_{\text{sa}}}}. \tag{2.13}$$

The rate of change of arterial volume can be related to the compliance and transmural pressure:

$$\frac{dV_{\text{sa}}}{dt} = \frac{d(C_{\text{sa}}(P_{\text{sa}} - P_{\text{ic}}))}{dt}. \tag{2.14}$$

The conservation of volume at the nodes enables to calculate the pressure in the haemodynamic model:

$$\frac{dP_{\text{sa}}}{dt} = \frac{1}{C_{\text{sa}}} \left(\frac{P_{\text{a}} - P_{\text{sa}}}{R_{la} + 0.5R_{\text{sa}}} - q - \frac{dC_{\text{sa}}}{dt}(P_{\text{sa}} - P_{ic}) \right), \tag{2.15}$$

$$\frac{dP_3}{dt} = \frac{1}{C_v} \left(q - \frac{P_3 - P_v}{R_{lv}} \right). \tag{2.16}$$

The total blood volume CBV can then be calculated as a sum of all compartmental volumes:

$$\text{CBV} = \text{V}_A + \text{V}_{\text{V}} + \text{V}_{\text{net}} \tag{2.17}$$

where arterial volume V_A and network volume V_{net} are calculated from:

$$V_A = V_{\text{la}} + V_{\text{sa}}, \tag{2.18}$$

$$V_{\text{net}} = \sum_{i=1}^{13} V_{b,i} \cdot N. \tag{2.19}$$

2.2.3. Network model

The network model proposed here is based upon the one introduced by Payne and Lucas (2018) and is a bifurcating vessel model consisting of 13 vessel generations (6 arteriolar, 1 capillary and 6 venous). One of the aims of the network was to represent all the generations of blood vessels responsible for oxygen delivery. Values of all characteristic vessel parameters can be found in table A1 in the appendix.

2.2.4. Oxygen supply

Within the vessels, oxygen is transported via convection and diffusion whereas in tissue it occurs solely via diffusion. Following the methods described by Payne and Lucas (2018), it was assumed that each vessel supplies a separate tissue voxel, with diffusion between these volumes being neglected. The governing equations for oxygen delivery follow:

$$V_b \frac{1}{2}\left(\frac{dS_{\text{in}}}{dt} + \frac{dS_{\text{out}}}{dt}\right) + \frac{1}{2}(q_{\text{in}} + q_{\text{out}})(S_{\text{out}} - S_{\text{in}}) = -\frac{2\pi KrL}{\text{hc}_{\text{Hb}}H}\left(\frac{1}{2}(p_{\text{in}} + p_{\text{out}}) - p_{\text{t}}\right) \tag{2.20}$$

$$\frac{dp_t}{dt} = \frac{1}{\alpha_t V_t}\left(\frac{2\pi KrL}{h}\left(\frac{1}{2}(p_{\text{in}} + p_{\text{out}}) - p_t\right) - MV_t\right), \tag{2.21}$$

where V_b is the blood volume, V_t is the supplied tissue volume, S_{in} and S_{out} are inlet and outlet saturation, q_{in} and q_{out} are inlet and outlet flow, r is the vessel radius, L is the vessel length, K is oxygen permeability of vascular wall, p_{in} and p_{out} are inlet and outlet vessel pressure, p_t is tissue partial pressure, M is oxygen metabolism of brain tissue, H is hematocrit and h is vessel wall thickness. The vessel blood volume results from:

$$V_b = \pi r^2 L. \tag{2.22}$$

Balancing the oxygen transfer from each vessel with the metabolic demand of the supplied tissue volume and if each vessel supplies an independent tissue voxel, the supplied volume V_t is given as:

$$V_t = \frac{c_{\text{Hb}} H \bar{q} \overline{\Delta S}}{M}, \tag{2.23}$$

where c_{Hb} is the oxygen carrying capacity per unit volume of red blood cells. The relationship introduced by Severinghaus (1979) was used to relate partial pressure and O_2 saturation in the blood:

$$S_{O_2} = \frac{1}{\left(1 + \left(\frac{23400}{p_b^3 + 150p_b}\right)\right)}. \tag{2.24}$$

The total volume of tissue supplied was obtained by computing the total sum of the product of the volume of the supplied voxel and the number of vessels within the generation. The volume averaged partial tissue pressure at baseline conditions was thus obtained as follows:

$$\langle \overline{p_t} \rangle = \sum_{i=1}^{13} \frac{p_{t,i} V_{t,i}}{\sum_{i=1}^{13} V_{t,i}}. \tag{2.25}$$

2.3. Feedback mechanisms

The compliance of small arteries was defined by the feedback mechanism assumed to control cerebral blood flow. Hence, the variables driving the feedback determined the model's response. With the aim of investigating the time response of the model, the efficacy of the flow-feedback was compared to three types of metabolic-feedback. The first variation of metabolic feedback relies solely on an oxygen-sensitive arterial compliance, the second includes pericyte activity on a capillary level and the third adds the role of neural activation.

2.3.1. Flow

The flow dependent feedback x_q, is given by the commonly used formulation (Payne 2006).

$$\tau_q \frac{dx_q}{dt} = -x_q + G_q\left(\frac{q - \bar{q}}{\bar{q}}\right), \tag{2.26}$$

where τ_{q} is a time constant and G_{q} is a scaling factor. The role of the time constant was to introduce a delay in the response, since changes in flow q are a by-product of chemical stimuli. The compliance of small arteries C_{sa} is therefore a sigmoidal curve whose behavior is governed by changes of flow. Ultimately, the sign of x_q determined whether the amplitude of compliance change was positive (ΔC_{sa}^{+}) or negative (ΔC_{sa}^{-}).

$$C_{\text{sa}} = \overline{C_{\text{sa}}} + \frac{1}{2}\Delta C_{\text{sa}}^{\pm} \tanh\left(\frac{2x_q}{\Delta C_{\text{sa}}^{\pm}}\right). \tag{2.27}$$

2.3.2. Oxygen

A novel equation for arterial compliance was developed, in order to relate its changes to variations in oxygen partial tissue pressure. The oxygen tissue partial pressure was then assumed to be related to changes in arterial compliance, yielding a model whose active response of the vasculature depends on changes in oxygen saturation

in the tissue. Unlike the flow-dependent compliance, the oxygen-sensitive arterial compliance had an immediate response. No time constant was introduced, as the aim was to define the fastest possible response time for oxygen sensitivity:

$$C_{sa} = \overline{C_{sa}} + \frac{1}{2}\Delta C_{sa}^{\pm} \tanh\left(\frac{\langle \overline{p_t} \rangle - \overline{p_t}}{p_s}\right), \tag{2.28}$$

where the amplitude of the compliance changed depending on the difference between the volume averaged partial tissue pressure $\langle \overline{p_t} \rangle$ and the baseline value of partial tissue pressure $\overline{p_t}$. If $(\langle \overline{p_t} \rangle - \overline{p_t}) > 0$ then the amplitude was ΔC_{sa}^{+} otherwise it was ΔC_{sa}^{-}. The magnitude of the scaling factor p_s was set to 10% of $\overline{p_t}$ to allow for a continuous plateau in the sigmoidal of the compliance function.

2.3.3. Oxygen and pericytes

The contribution of the pericytes was accounted for as capillary dilation induced by Ca^{2+} stimuli. To include pericyte-induced vasodilation in the capillaries the model fit was imposed as a diameter variation of the capillaries. This response was assumed to be directly linked to a variation in arterial blood pressure (ABP) from the baseline condition. The percentage of responding vessels was assumed to be 75%, based on previous experimental studies (Hall *et al* 2014). As the partial tissue pressure is a function of the vessel diameter, the compliance of the network C_N can therefore be expressed following the same principles defined in equation (2.28):

$$C_N = \overline{C_N} + \frac{1}{2}\Delta C_{sa}^{\pm} \tanh\left(\frac{\langle \overline{p_t} \rangle - \overline{p_t}}{p_s}\right), \tag{2.29}$$

where $\overline{C_N}$ is the baseline value of the network's compliance and the amplitude ΔC_N is positive if $(\langle \overline{p_t} \rangle - \overline{p_t}) > 0$ and is negative if $(\langle \overline{p_t} \rangle - \overline{p_t}) < 0$.

2.3.4. Neural activation

The neural activity variable included in the model was linked to the $CMRO_2$ variation recorded in the imaged tissue region. It was experimentally determined that the time delay in the response was about 1 s, which was introduced in the neural activation function as a $\tau = 1$ s delay. Using a second order dynamic model, neural activation was represented as:

$$\frac{d^2 x_n}{dt} = \frac{1}{\tau}\left(n - \tau^2 \frac{dx_n}{dt} - x_n\right), \tag{2.30}$$

where $n = 0.4$ is the parameter signaling neuronal activity. Here, neural activation acts in addition to the oxygen sensitivity and the pericyte activity and the compliance of the network can therefore be defined as:

$$C_N = \overline{C_N} + \frac{1}{2}\Delta C_{sa}^{\pm} \tanh\left(\frac{\langle \overline{p_t} \rangle - \overline{p_t}}{p_s} + x_n\right), \tag{2.31}$$

where $\overline{C_N}$ is the baseline value of the network's compliance and the amplitude ΔC_N was positive if $(\langle \overline{p_t} \rangle - \overline{p_t}) > 0$ and was negative if $(\langle \overline{p_t} \rangle - \overline{p_t}) < 0$.

3. Results

Pericyte activity was quantified in terms of capillary dilation magnitude and response time. These experimental results were then included in the model's dynamic regulation of flow. Finally, the computational vascular model was studied under static and dynamic conditions and its outputs were compared to existing models.

3.1. Pericyte activity induces a 2.5% capillary dilation

The vessel diameters of all 26 vessels range between 2 and 13 μm, as shown in figure 2. Figure 3 illustrates an example of data processing for V1, where a sequential Ca^{2+} stimulus induced a repeated diameter change of about 6%. An average capillary dilation was computed for all 26 vessels and compared to the average dilation of the 8 relevant vessels, selected following the criteria outlined in the section 2.1.2. Figure 4 shows that the average pericyte-induced capillary dilation for all 26 vessels is 1.25% compared to 2.65% for the 8 selected vessels and that the response time is about 1 s. Table A1 in the appendix presents data on the 12 responsive capillary vessels.

3.1.1. Diameter trace function

Figure 5(a) shows the model fit to the diameter trace for capillaries with a diameter between 6 and 10 μm. The time constants $\left(T_\alpha = \frac{1}{\alpha},\ T_\beta = \frac{1}{\beta},\ T_\gamma = \frac{1}{\gamma}\right)$ and gain were calculated to be: $T_\alpha = 33.33$ s, $T_\beta = 2.38$ s, $T_\gamma = 0.90$ s

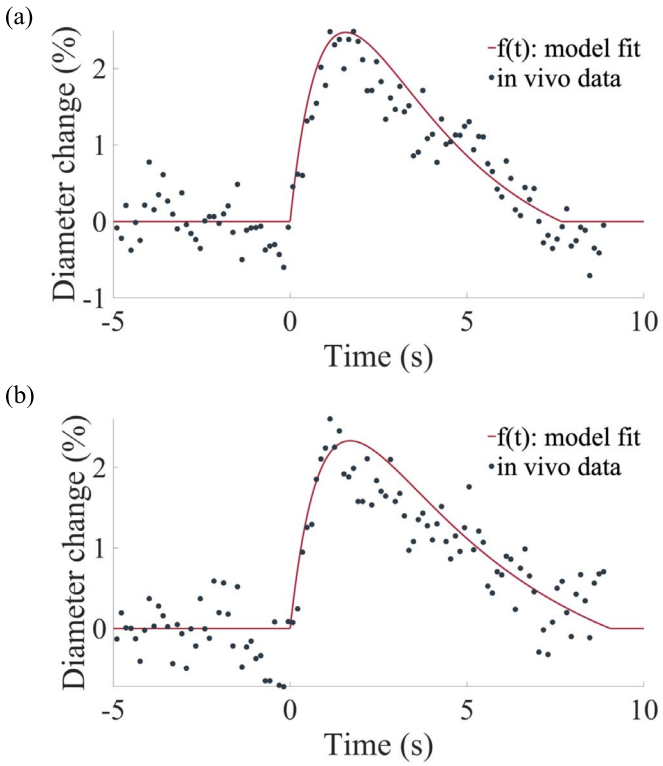

Figure 5. Model fit of capillary dilation for (a) large (6–10 μm) and (b) small (2–6 μm) vessels.

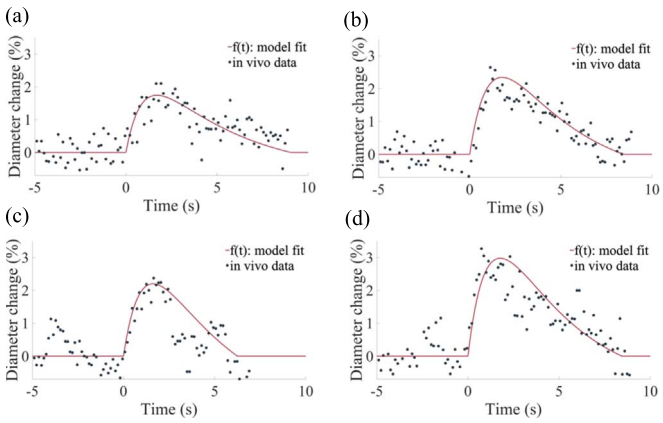

Figure 6. Model fit for depth-dependent capillary dilation where: (a) 0–50 μm, (b) 50–150 μm, (c) 150–250 μm and (d) 250–350 μm.

and $K = 4.8$. The fitted function shows a maximum diameter variation of 2.51% from the baseline value and a time response about 1 s. Figure 5(b) shows the result of the model fit for capillaries whose diameter ranges 2–6 μm. The parameters defining the Laplacian are: $T_\alpha = 20.02$ s, $T_\beta = 5.01$ s, $T_\gamma = 0.90$ s and $K = 4.0$. The peak dilation of the model fit is 2.34% and the response time is about 2 s.

3.1.2. Response time increases with depth

The collected data are from a wide range of imaging depths 0–350 μm. To investigate the depth-dependent dilation properties of pericytes, the total range was divided into 4 categories: 0–50, 50–150, 150–250 and 250–350 μm. Figures 12–15 in the appendix show the imaged capillary dilation for each vessel depth category. Figure 6 shows that there are slight differences in peak dilation at different imaging depths. It is worth noting that the vessel number and diameter differ for each depth category.

Table 1 Summarizes the depth-dependent vessel classification and table 2. Summarizes the respective imaging depth time constant parameters, the mean values, standard deviations and error bars. The linear regression, p-value and R-squared values of each time constant are also included.

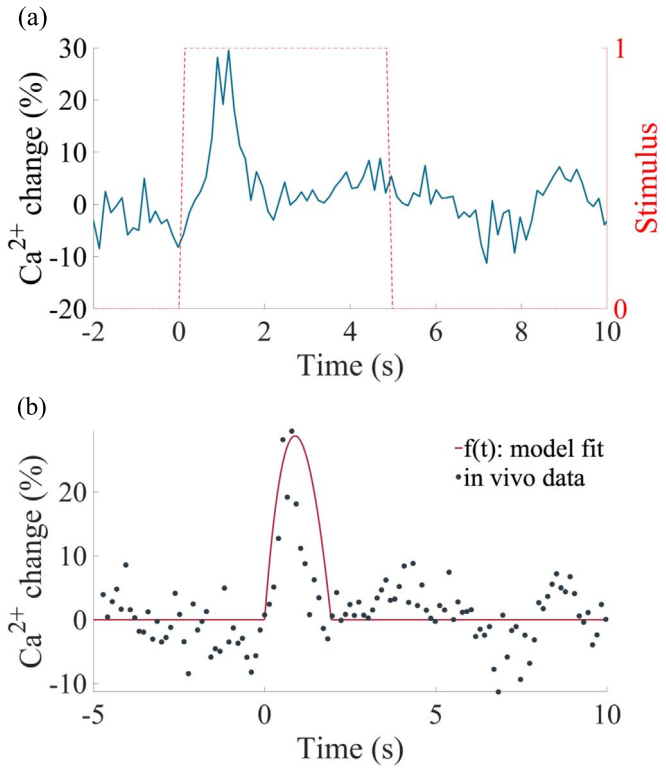

Figure 7. (a) Averaged Ca^{2+} trace; (b) fitted function to the Ca^{2+} trace for the eight vessels selected to be included in the computational model.

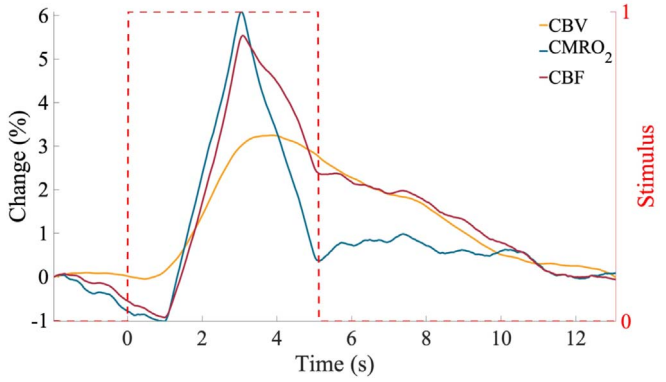

Figure 8. As a response to neural activation, signaled by the increase in Ca^{2+} in the tissue surrounding the vessel, CBV increases by 3.25% (yellow); $CMRO_2$ increases by 6.09% (blue); CBF increases by 5.53% (red).

3.1.3. Statistical significance

A statistical analysis was performed to investigate the differences in response to Ca^{2+} stimuli, between large capillaries (6–10 μm diameter) and small capillaries (2–6 μm diameter) and imaging depths:

- **Diameter significance**
  A statistical analysis (two sample *t*-test) showed that there is a statistically significant difference p=0.034 between the peak dilation of the large and small capillary vessels.
- **Imaging depth significance**
  It was shown that the response of vessels also differs for various imaging depths. To compare four groups of imaging depths the ANOVA test was applied. A statistically significant difference was proven $p < 0.001$. A post-hoc analysis showed that all groups are statistically different from each other.
- **Time constants variation**

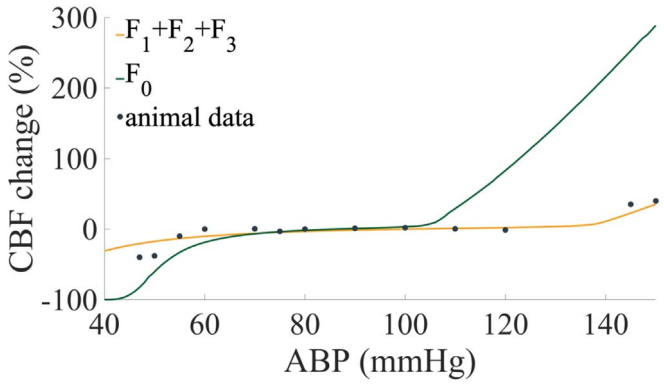

Figure 9. (a) Flow feedback-based CA model; (b) oxygen, pericytes and neural feedback-based ($F_1 + F_2 + F_3$) CA model fitted against experimental data reported by Ursino (1998).

The *t*-test was performed in order to investigate the statistical significance of the difference of the time constant parameters in the small and large capillary vessels. The comparison of the T_α time constants revealed no statistical significance ($p = 0.53$), T_β yielded a positive statistical significance ($p = 0.025$), whereas T_γ resulted in no statistical significance ($p = 0.35$). This suggests that compared to large capillaries (6–10 μm diameter), the smaller capillaries (2–6 μm diameter) have an overall slower response time.

3.1.4. Calcium trace

An analogous analysis was performed for the Ca^{2+} stimuli peak detection and response time. Figure 7(a) shows the Ca^{2+} trace for the eight selected vessels and figure 7(b) illustrates the function fit for the Ca^{2+} data points.

3.1.5. Capillary $CMRO_2$, CBF and CBV

As capillaries increase in diameter, so does the blood flow and volume. Figure 8 illustrates how the 2.5% increase in vessel diameter corresponds to a 5.53% increase in CBF, a 3.25% increase in CBV and a 6.09% increase in $CMRO_2$. The relationship between CBF and CBV was defined by Grubb as:

$$\mathrm{CBV} = 0.8 \cdot \mathrm{CBF}^{\alpha}, \tag{3.1}$$

where α is Grubb's exponent whose original value is 0.38. Given that this value was derived from rhesus monkeys, a number of studies have attempted to find a better fit for relating the two parameters in humans. At present, there is still a lack of consensus and the proposed values range from 0.29 (Ito *et al* 2005) to 0.73 (Rostrup *et al* 2005). Here, the value used for α is 0.73, to best fit the relationship between CBV and CBF, where the increase in volume corresponds to about half the increase in flow.

To investigate the $CMRO_2$ change in the parenchyma around the capillary, resulting from the visual stimuli-induced increase in Ca^{2+} concentration, an average response was computed from the total of all stimuli across the 36 vessels. As outlined in section 2.1, this second data set was used to study changes in oxygen metabolism, as changes in CBF and changes in vessel diameter cannot be measured simultaneously.

3.2. Model simulations

The ability of the four feedback mechanisms to physiologically accurately replicate CBF regulation for variations of ABP, was evaluated under static and dynamic conditions. In the steady state, CBF was maintained constant over a wide range of ABP (40–150 mmHg) while in the dynamic state, a 10% increase in ABP resulted in a 20%–35% temporary increase in CBF, depending on the feedback mechanism that was used.

3.2.1. Steady state cerebral autoregulation (CA)

Solving the equations under steady state conditions, the change of CBF was observed over a wide range of ABP (40–150 mmHg). All four feedback mechanisms proved to be in good agreement with the literature (Ursino *et al* 1998) as CBF was maintained constant between 60 and 120 mmHg (see figure 9). The models showed however a clear difference in the range of the upper and lower autoregulation limit. The arterial compliance of the flow feedback model clearly saturated more promptly, resulting in a sudden drop in flow below 60 mmHg of ABP and a rapid increase above 120 mmHg of ABP. In comparison, the range of autoregulation of the oxygen and pericyte feedback model is larger, stretching from about 50 mmHg to 140 mmHg. Frequently cited data of cats and mice (Ursino *et al* 1998) were used to validate the steady state ($F_1 + F_2 + F_3$) feedback model. It should be noted that

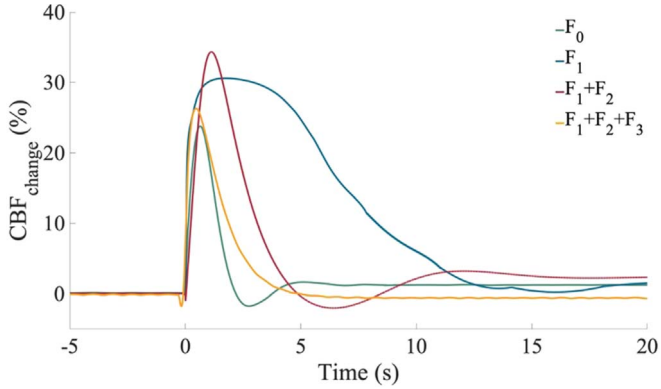

Figure 10. CBF variation upon a 10% increase in ABP for 4 scenarios: a flow feedback (F_0), an oxygen-feedback (F_1), an oxygen and pericytes feedback ($F_1 + F_2$), and an oxygen, pericytes and neural feedback ($F_1 + F_2 + F_3$).

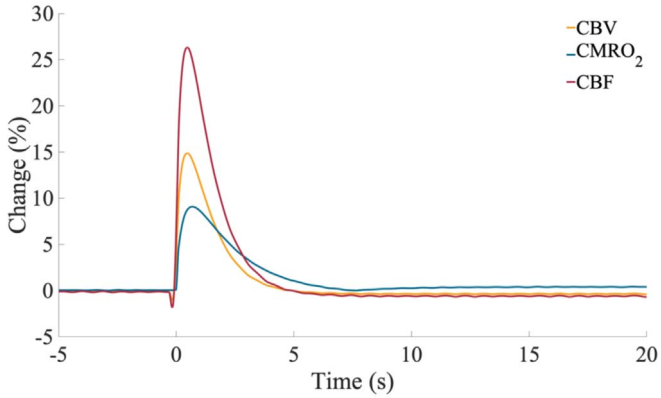

Figure 11. CBF, $CMRO_2$ and CBV variation upon a 10% increase in ABP.

the upper and lower autoregulation limits strongly depend on the parameters of the compliance equation. The passive presence of pericytes was also studied by imposing a maximum increase in capillary diameter (2.5%), derived from the fitted function in section 3.1. The steady state analysis showed no statistically significantly different behavior compared to the active based one.

3.2.2. Dynamic CBF regulation

To further investigate the physiological accuracy of the proposed computational model, the time response was evaluated for each of the four feedback mechanisms. Indeed, the rapidity of the response can serve as an indicator for the overall ability of each regulatory variable (oxygen, pericytes and neurons) in regulating CBF when ABP changes. To investigate the time response to changes in oxygen partial tissue pressure, the governing equations of the model were solved under dynamic conditions and a 10% increase in ABP was imposed at time $t = 0$ s of the solver (see figure 10).

At the time of the impulse, CBF increased by 23.79% in the flow-based model (F_0), by 30.58% in the oxygen-based model (F_1), by 34.33% in the model including pericytes ($F_1 + F_2$) and by 26.32% in the one including neural activation ($F_1 + F_2 + F_3$). The time responses of CBF are 2.3 s for the flow based, 10.8 s for the oxygen based, 5.8 s for the oxygen and pericyte driven model and 4.1 s when neural activity is included as a further CBF regulator.

The dynamic response of the blood volume compartments was evaluated under the same conditions. The computational model has shown that the arterial volume V_A rises by 11.98% at the moment of the impulse, while the venous volume V_V rises by 2.76% before settling to baseline condition. The sum of both volume compartments yields the total CBV whose impulse response shows an increase of 14.88%. Finally, as a result of the 10% increase in ABP which resulted in a 26.32% increase in CBF, the model calculated a 9.10% increase in $CMRO_2$ (see figure 11).

Table 1. Imaging depth-dependent vessel classification.

Diameter (6–10 μm)				
Imaging depth	0–50 μm	50–150 μm	150–250 μm	250–350 μm
Vessel	—	V4, V15, V22	V11, V16, V23	V1, V18
Peak dilation (%)	—	2.42	2.37	3.2
Diameter (2–6 μm)				
Imaging depth	0–50 μm	50–150 μm	150–250 μm	250–350 μm
Vessel	V13	V2, V7, V24	—	—
Peak dilation (%)	2.1	2.79	—	—

Table 2. Mean values μ, standard deviations σ and error-bars for each time constant per imaging depth category; individual time constant data analysis reporting the p-value, R-squared, R-squared adjusted and root mean square error (RMSE).

Depth	0–50 μm	50–150 μm	150–250 μm	250–350 μm
$\mu_{1/\alpha}$	20.0	20.0	10.0	20.0
$\mu_{1/\beta}$	5.0	4.0	4.0	4.0
$\mu_{1/\gamma}$	0.90	1.11	1.11	1.11
$\sigma_{1/\alpha}$	0	4.35	2.15	0
$\sigma_{1/\beta}$	0	0.86	2.11	0.47
$\sigma_{1/\gamma}$	0	0.25	0.16	0
$\mathrm{err}_{1/\alpha}$	0	1.77	1.24	0
$\mathrm{err}_{1/\beta}$	0	0.22	1.21	0.33
$\mathrm{err}_{1/\gamma}$	0	0.06	0.09	0
Variable	*p*-value	R^2	R^2-adjusted	RMSE
T_α	0.062	0.30	0.24	3.85
T_β	0.44	0.06	−0.034	1.16
T_γ	0.40	0.07	−0.02	0.27
K	0.24	0.14	0.05	0.98

4. Discussion

A new mathematical model of cerebral autoregulation was presented here. Four feedback mechanisms modeling approaches (F_0, F_1, $F_1 + F_2$ and $F_1 + F_2 + F_3$) were compared for the modeling of CBF regulation. The first is a flow feedback-based model, the second a solely oxygen sensitivity signaling, the third is an oxygen and pericyte based feedback mechanism and the fourth included neural activity as a further CBF regulator. The peak dilation for capillaries with a large diameter (6–10 μm diameter) was found to be a 2.51% increase from the vessel's baseline value, the response time being about 1 s. In comparison, smaller capillaries (2–6 μm diameter) responded with a peak dilation of 2.34% and a time response of about 2 s. The comparison of the response of both vessel groups proved to be statistically significant. The differences in capillary dilation for vessels imaged at different depths was also studied and was found to be statistically significant. Indeed, capillary vessels found in deeper cortical layers expressed a longer response time and a greater dilation (see figure 6). This difference in dilation magnitude could be attributed to the fact the deeper cortical layers are more active, therefore capillaries might be required to dilate more in order to supply the tissue with a high nutrient demand. To validate this hypothesis, further analysis with a higher number of vessels should be conducted, in order to be able to surely conclude that larger capillaries found in the deeper layers of the cortex (150–350 μm depth) have a greater dilation potential than capillaries found in more superficial layers of the cortex (0–150 μm depth).

Under steady state conditions, all feedback scenarios proved to be in good agreement with experimental data (see figure 9). The differences in feedback mechanisms were highlighted by the dynamic analysis (see figure 10). It was found that metabolism alone (i.e. oxygen sensitivity) is insufficient for a rapid CBF regulation, and that including pericytes and neural activation improved agreement physiological reality. In a healthy brain, CBF is maintained by the autoregulatory mechanism of vasoconstriction and vasodilation when the cerebral perfusion pressure (CPP) is increased or decreased respectively. Hence, during autoregulation while CBF is maintained constant, the drop in CBV is compensated by the cerebrovascular reserve. When CPP surpasses the upper limit

of autoregulation, CBF increases as a result. Alternatively, when CPP decreases below the lower limit of autoregulation, CBF decreases. Low CPP below the limit of autoregulation results in a decrease in CBF with an increase in the oxygen extraction fraction, which is necessary to maintain $CMRO_2$.

$CMRO_2$ and CBF changes were also quantified experimentally. As a result of neural activation, $CMRO_2$ was found to increase by 6.09% from its baseline value within 2 s of the stimulation. CBF increased by 5.53% from baseline after about 3 s since the start of the stimulation (see figure 8).

Changes in oxygen content within the tissue have shown to be slow relative to the changes in blood flow. Within the macro-vasculature, this indicates a low sensitivity of SMC to changes in oxygen concentration of the surrounding tissue. Moreover, in a whole brain mathematical model, it was found that for each percentage increase in CBF, about a third of the increase in $CMRO_2$ is shown (see figure 11). This result differs when considering an individual vessel of the microvasculature experimentally and possibly even the microvasculature network in its entirety. Here, the changes of oxygen metabolism occur at a much faster rate (2 s compared to the 10.8 s in a whole brain model) and the ratio of CBF to $CMRO_2$ change is 1:1. This could be justified by the activity of pericyte cells, whose proximity to the neurons ensures a fast change in vessel diameter. Moreover, a faster response of microvasculature compared to large arteries and veins, supports the now widespread notion that the first stage of blood flow regulation in response to metabolic and myogenic stimuli occurs within the microvasculature (Blanco *et al* 2017, Sweeney *et al* 2018).

A limitation of the experimental validation of this study is the impossibility of measuring changes in $CMRO_2$ in the tissue and changes in capillary diameter simultaneously. Indeed, the experimental methods available for the study of the effect of visual stimulation in mice, can only image either $CMRO_2$/Hb or Ca^{2+}/vasomotion. This results in two sets of data, obtained in different instances, to be compared with each other. Although the experimental procedure is the same in both scenarios, the inability of monitoring all the variables within the same measurement is to be noted.

Finding the right balance between physiological accuracy and computational feasibility is always a challenge. Hence, three computational limitations of the model need to be mentioned. Firstly, no oxygen diffusion between tissue compartments was considered. Each vessel supplies an individual and independent tissue volume. Including nutrient exchange between volume voxels would possibly decrease the response time further yet this is still to be explored and is significantly harder to implement and validate with adequate experimental data. Secondly, the number of pericytes considered for the model fit is very low and these are from animal models. While the pericyte to endothelial cell ratio (1:3) is the same for mice and humans (Hall *et al* 2014), the use of animal data in a human brain model is to be noted. Thirdly, there is no spatial information on the oxygen distribution within the microvasculature. Studies (Shaw 2019) have shown that there are regional differences in oxygen distribution within the tissue, suggesting that some parts of the capillary network might be more active than others depending on their location within the brain.

5. Conclusion

Currently existing mathematical models of cerebral blood flow autoregulation are flow feedback based. Despite the fact that such models provide results that can be validated with experimental data, the nature of the feedback is not physiologically accurate. In order to be clinically significant, new mathematical models need to be designed. Such models could indeed be of aid for patients under continuous monitoring, as they could provide clinicians with a clearer insight into which of the numerous parameters influencing CBF regulation need adjustment.

Numerous studies have suggested that pericytes may be an additional regulating factor of blood perfusion. They act on the capillary bed, constricting or dilating capillary vessels in response to chemical stimuli (e.g. Ca^{2+} concentration variations). Data on Ca^{2+} concentration-induced capillary diameter variation were collected and subsequently analyzed here. It was found that the average maximum dilation of capillaries is of 2.51% from their baseline diameter.

In the steady state analysis, all four feedback mechanisms were found to be maintaining CBF over a wide range of ABP. Their differences, however, were highlighted when the dynamic response of CBF to changes in ABP was analyzed. An increase of 10% of ABP was induced and the response of the vasculature was observed. It was found the response time of the flow feedback model is 2.3 s whilst that of the oxygen feedback based one is 10.8 s, that of the oxygen and pericytes based one is 5.8 s and that by including neural activity as an additional CBF regulator, the response time decreases to 4.1 s. These findings highlight the essential role of an active microvasculature for a rapid CBF regulation. In particular, this study indicates that pericytes do indeed play a significant role in CBF regulation, as oxygen sensitivity alone results in a response that is too slow to be physiologically accurate.

Appendix

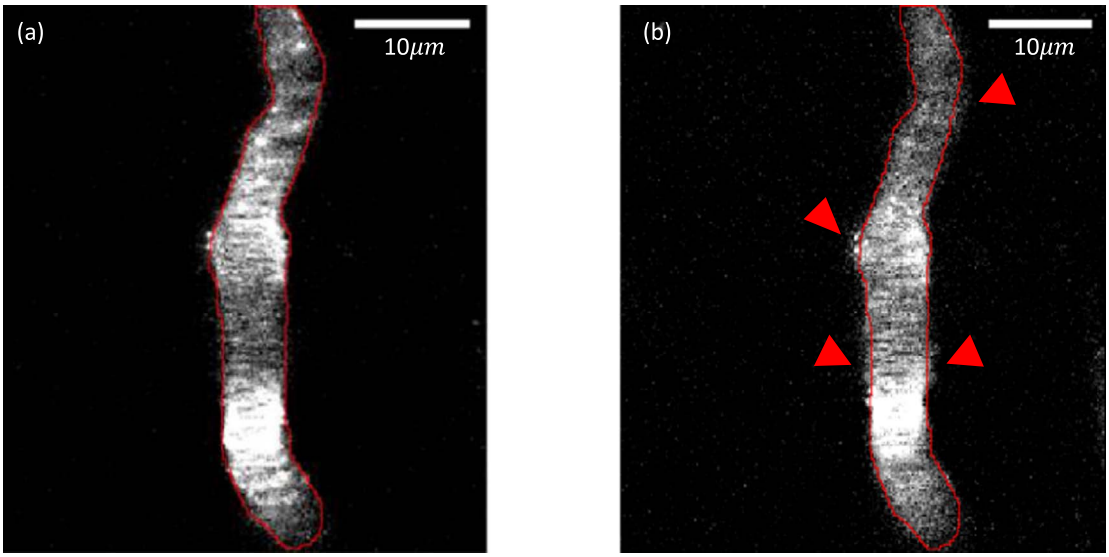

Figure 12. Capillary vessel imaged at 0–50 μm depth, where (a) shows the vessel at rest and (b) shows the vessel dilation. To facilitate visualization, the red line outlines the vessel wall at rest and the red triangles direct attention towards the areas of dilation.

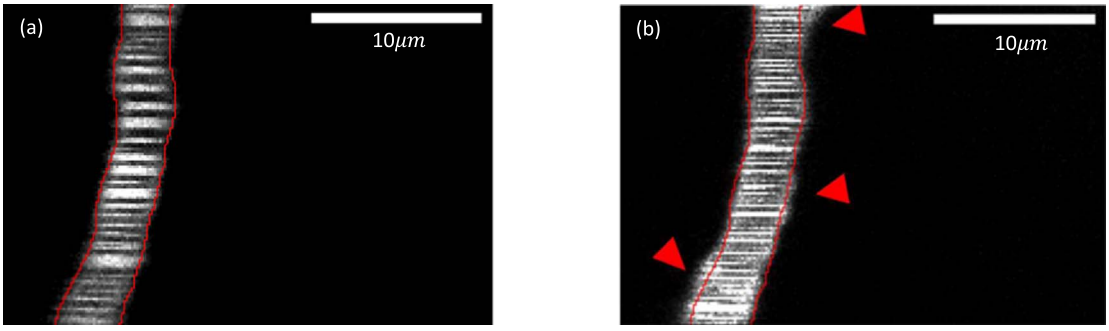

Figure 13. Capillary vessel imaged at 50–150 μm depth, where (a) shows the vessel at rest and (b) shows the vessel dilation. To facilitate visualization, the red line outlines the vessel wall at rest and the red triangles direct attention towards the areas of dilation.

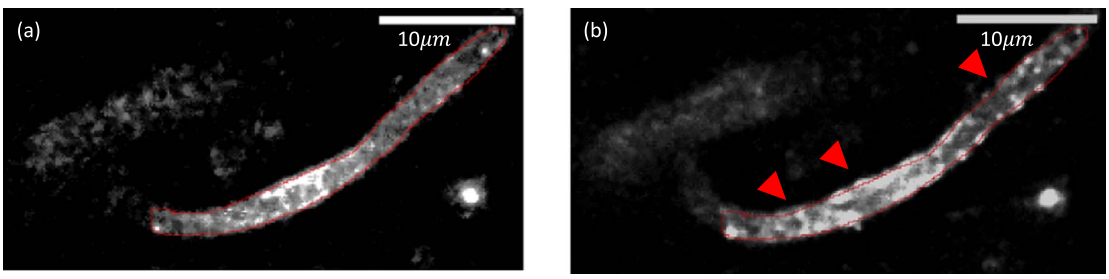

Figure 14. Capillary vessel imaged at 150–250 μm depth, where (a) shows the vessel at rest and (b) shows the vessel dilation. To facilitate visualization, the red line outlines the vessel wall at rest and the red triangles direct attention towards the areas of dilation.

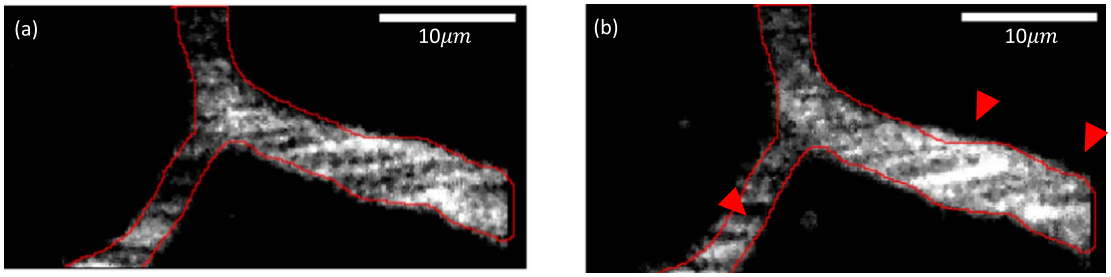

Figure 15. Capillary vessel imaged at 250–350 μm depth, where (a) shows the vessel at rest and (b) shows the vessel dilation. To facilitate visualization, the red line outlines the vessel wall at rest and the red triangles direct attention towards the areas of dilation.

Table A1. Comprehensive table of baseline capillary vessel diameters and dilation, depth and time constants for relevant vessels, where D is the diameter, Dch is the diameter change, d is the depth, CV is the coefficient of variance and $1/\alpha$, $1/\beta$, $1/\gamma$ and K are the time constants of the fitted function.

Vessel	D(μm)	Dch(%)	d(μm)	CV(%)	$1/\alpha$ (s)	$1/\beta$ (s)	$1/\gamma$ (s)	K
V1	7.26	3.6	257.7	0.86	10.0	4.0	1.43	4.5
V2	3.28	3.0	138.5	0.42	20.0	5.0	1.42	3.7
V3	7.77	—	—	—	—	—	—	—
V4	6.67	3.4	137.8	0.61	16.66	3.33	1.66	4.0
V5	7.02	—	—	—	—	—	—	—
V6	12.94	—	—	—	—	—	—	—
V7	3.39	2.6	142.6	0.77	20.0	5.0	1.25	3.7
V8	6.78	—	—	—	—	—	—	—
V9	4.08	—	—	—	—	—	—	—
V10	5.13	—	—	—	—	—	—	—
V11	6.61	2.1	158.4	0.37	12.5	4.0	1.11	3.0
V12	6.62	—	—	—	—	—	—	—
V13	3.12	2.5	0	0.37	20.0	5.0	0.90	3.0
V14	6.84	—	—	—	—	—	—	—
V15	6.10	3.4	92.9	1.15	20.0	5.0	1.11	3.7
V16	7.86	3.2	142.2	0.98	10.0	2.5	1.11	6.0
V17	4.66	—	—	—	—	—	—	—
V18	8.14	3.5	345.4	1.08	10.0	3.33	1.43	4.7
V19	6.69	—	—	—	—	—	—	—
V20	6.68	—	—	—	—	—	—	—
V21	6.07	—	—	—	—	—	—	—
V22	6.84	1.4	149.5	0.32	11.11	5.0	1.11	2.0
V23	9.01	2.2	153.4	1.22	14.28	6.66	0.83	3.5
V24	4.45	3.0	65.2	0.68	11.11	3.33	1.66	4.0
V25	4.34	—	—	—	—	—	—	—
V26	2.08	—	—	—	—	—	—	—

Table A2. Constant parameters and baseline values of the variables that define the novel mathematical model.

Variable	Magnitude	Definition	Source
N	$3.38 \cdot 10^{6}$	Number of parallel vessels	—
k	$2.96 \cdot 10^{-7}$	Scaling factor (1/N)	—
$\bar{q}$	12.5 · k (ml)	Baseline CBF	Payne (2006)
$\overline{C_{sa}}$	0.125 · k (ml/mmHg)	Baseline compliance of SA	Payne (2006)
$\Delta C_{sa}{}^{+}$	2.87 · k	Amplitude of + change of C_{sa}	Payne (2006)
$\Delta C_{sa}{}^{-}$	0.164 · k	Amplitude of - change of C_{sa}	Payne (2006)
R_{la}	0.40 · N (mmHg s/ml)	Resistance of large arteries	Payne (2006)
R_{lv}	0.56 · N (mmHg s/ml)	Resistance of large veins	Payne (2006)
$\overline{R_{sa}}$	5.03 · N (mmHg s/ml)	Baseline resistance of small arteries	Payne (2006)
R_{sv}	1.18 · N (mmHg s/ml)	Resistance of small veins	Payne (2006)
R_N	$2.98 \cdot 10^{-5}$ · N (mmHg s/ml)	Microvasculature resistance	—
$\overline{P_v}$	6 (mmHg)	Baseline venous pressure	Payne (2006)
P_{ic}	10 (mmHg)	Intracranial pressure	Payne (2006)
P_{v1}	-2.25 (mmHg)	Venous compliance pressure offset	Payne (2006)
P_{net}	25 (mmHg)	Network outlet pressure	Payne and Lucas (2018)
$\overline{P_t}$	38.1 (mmHg)	Baseline O2 partial pressure	—
V_{la}	1 · k (ml)	Volume of large arteries	Payne (2006)
$\overline{V_{sa}}$	12 · k (ml)	Baseline volume of small arteries	Payne (2006)
V_{vn}	28 · k (ml)	Venous volume offset	Payne (2006)
V_{TotNet}	$8.56 \cdot 10^{-6}$ (ml)	Total network volume	—
V_{aNet}	$2.17 \cdot 10^{-6}$ (ml)	Network arterial volume	—
V_{vNet}	$5.63 \cdot 10^{-6}$ (ml)	Network venous volume	—
V_{cNet}	$7.84 \cdot 10^{-7}$ (ml)	Network capillary volume	—
k_{ven}	0.186/k (1/ml)	Venous elastance coefficient	Payne (2006)
c_{Hb}	0.2 mlO_2 (1/ml)	O2 carrying capacity/unit volume	Payne and Lucas (2018)
α_t	$2.6 \cdot 10^{-5}$ (mlO_2/ml.mmHg)	O2 solubility in brain tissue	Payne and Lucas (2018)
M	$30 \cdot 10^{-9}/4.46 \cdot 10^{-5}$ (mlO_2/ml)	O2 metabolism	Payne and Lucas (2018)
K	$5 \cdot 10^{-11}$(ml/mm.s.mmHg)	O2 permeability of vascular wall	Payne and Lucas (2018)
H	0.42	hematocrit	Payne (2006)
ρ	1040 (kg m^{-3})	Blood density	Payne (2006)
E	$1600 \cdot 10^{3}$ (Pa)	Young modulus	Payne and El-Bouri (2017)
ν	$3 \cdot 7.5 \cdot 10^{-6}$ (mmHg.s)	Kinematic viscosity	Payne and El-Bouri (2017)

ORCID iDs

Catherine Hall https://orcid.org/0000-0002-2316-7714

References

Attwell D, Mishra A, Hall C N, Farrell F M O and Dalkara T 2016 What is a pericyte? *J. Cerebral Blood Flow Metab.* **36** 451–5

Banaji M, Tachtsidis I, Delpy D and Baigent S 2005 A physiological model of cerebral blood flow control *Math. Biosci.* **194** 125–73

Bessonov N, Sequeira A, Simakov S, Vassilevskii Y and Volpert V 2016 Methods of blood flow modelling *Math. Modelling Nat. Phenom.* **11** 1–25

Blanco P J, Müller L O and Spence J D 2017 Blood pressure gradients in cerebral arteries: a clue to pathogenesis of cerebral small vessel disease *Stroke Vascular Neurol.* **2** 108–17

Bulte D P *et al* 2012 Quantitative measurement of cerebral physiology using respiratory-calibrated MRI *Neuroimage* **60** 582–91

Burdyga T and Borysova L 2014 Calcium signalling in pericytes *J. Vascular Res.* **51** 190–9

Bélanger M, Allaman I and Magistretti P J 2011 Brain energy metabolism: focus on astrocyte-neuron metabolic cooperation *Cell. Metab.* **14** 724–38

Cassot F and Lauwers F 2006 A novel three-dimensional computer-assisted method for a quantitative study of microvascular networks of the human cerebral cortex *Microcirculation* **13** 1–18

Cheng Y, Qin Q, van Zijl P C M, Pekar J J and Hua J 2017 A three-dimensional single-scan approach for the measurement of changes in cerebral blood volume, blood flow, and blood oxygenation-weighted signals during functional stimulation *Neuroimage* **147** 976–84

Cipolla M J 2016 The cerebral circulation *Colloquium Series on Integrated Systems Physiology: From Molecule to Function to Disease* vol 8 2nd edn (San Francisco, CA: Morgan & Claypool)

Hall C N *et al* 2014 Capillary pericytes regulate cerebral blood flow in health and disease *Nature* **508** 55–60

Ito H, Ibaraki M, Kanno I, Fukuda H and Miura S 2005 Changes in the arterial fraction of human cerebral blood volume during hypercapnia and hypocapnia measured by positron emission tomography *J. Cerebral Blood Flow Metab.* **25** 852–7

Payne S J 2006 A model of the interaction between autoregulation and neural activation in the brain *Math. Biosci.* **204** 260–81

Payne S J 2016 Cerebral autoregulation *Control of Blood Flow in the Brain* (Cham: Springer)

Payne S J and El-Bouri W 2018 Modelling dynamic changes in blood flow and volume in the cerebral vasculature *Neuroimage* **176** 124–37

Payne S J and Lucas C 2018 Oxygen delivery from the cerebral microvasculature to tissue is governed by a single time constant of approximately 6 s *Microcirculation* **25** 1–11

Reglin B, Secomb T W and Pries A R 2009 Structural adaptation of microvessel diameters in response to metabolic stimuli: where are the oxygen sensors? *Am. J. Physiol.-Heart Circ. Physiol.* **297** 2206–19

Rostrup E, Knudsen G M, Law I, Holm S, Larsson H B W and Paulson O B 2005 The relationship between cerebral blood flow and volume in humans *Neuroimage* **24** 1–11

Severinghaus J W 1979 Simple, accurate equations for human blood O_2 dissociation computations *J. Appl. Physiol.* **46** 599–602

Shaw K 2019 Hippocampus has lower oxygenation and weaker control of brain blood flow than cortex, due to microvascular differences *Nat. Commun.* at press (https://doi.org/10.1101/835728)

Sweeney M D *et al* 2019 Vascular dysfunction—the disregarded partner of Alzheimer's disease *Alzheimer's Dementia* **15** 158–67

Sweeney P W, Walker-samuel S and Shipley R J 2018 Insights into cerebral haemodynamics and oxygenation utilising *in vivo* mural cell imaging and mathematical modelling *Sci. Rep.* **8** 1–15

Ursino M and Lodi C A 1997 A simple mathematical model of the interaction between intracranial pressure and cerebral hemodynamics *J. Appl. Physiol.* **82** 1256–69

Ursino M *et al* 1998 Interaction among cerebral autoregulation, CO_2 reactivity and intracranial pressure : a mathematical model *Am. J. Physiol.-Heart and Circ. Physiol.* **274** 1715–28

Wintermark M *et al* 2005 Comparative overview of brain perfusion imaging techniques *Stroke* **36** e83–99